JOURNAL OF AIRCRAFT
Vol. 41, No. 4, July–August 2004

Studies on Vortex Flaps with Rounded Leading Edges for Supersonic Transport Configuration

Kenichi Rinoie* and Katsuhiro Miyata†
University of Tokyo, Tokyo 113-8656, Japan
and
Dong Youn Kwak‡ and Masayoshi Noguchi§
National Aerospace Laboratory, Tokyo 181-0015, Japan

Wind-tunnel measurements were taken on a cranked arrow wing supersonic transport configuration with leading-edge vortex flaps. Force and surface pressure measurements were made at Reynolds number based on the wing mean aerodynamic chord from 9.2×10^5 to 3.8×10^6. Two different flap cross sections (the originally designed nonrounded leading edge and the rounded leading edge) were tested. The purpose of the measurements is to clarify how the differences of the Reynolds number affect the flow around the rounded leading-edge vortex flaps and the flap performance. The wing with the rounded leading-edge vortex flaps indicated some benefit of the lift/drag ratio as compared with those of the nonrounded vortex flaps at a relatively high-lift coefficient greater than 0.3. Different flow patterns were observed over the rounded leading-edge vortex flaps when the Reynolds number was increased at a lift coefficient greater than 0.5. The spanwise length of the separated region shortens as the Reynolds number is increased.

Nomenclature

b	=	local span, m
$b_{\max}$	=	wing maximum span length, m
C_A	=	axial force coefficient
C_D	=	drag coefficient
C_L	=	lift coefficient
C_m	=	pitching moment coefficient nondimensionalized using C_{mac} and measured about 0.25 C_{mac}
C_{mac}	=	wing mean aerodynamic chord, m
C_p	=	pressure coefficient
C_r	=	wing root chord at model centerline, m
D	=	rounded leading-edge diameter, m
L/D	=	lift/drag ratio
M	=	freestream Mach number
Re	=	Reynolds number based on mean aerodynamic chord
U_∞	=	freestream velocity, m/s
x	=	chordwise coordinate measured from apex of delta wing at model centerline, m
y	=	spanwise coordinate orthogonal to x, measured from model centerline, m
α	=	wing angle of attack, deg
δ_{fLEin}	=	inboard vortex flap deflection angle, deg
δ_{fLEout}	=	outboard leading-edge flap deflection angle, deg

Presented as Paper 2002-8.7.3 at the 23rd International Council of the Aeronautical Sciences Congress (ICAS), Toronto, Canada, 8–13 September 2002; received 28 November 2002; revision received 13 June 2003; accepted for publication 16 June 2003.

*Associate Professor, Department of Aeronautics and Astronautics, 7-3-1 Hongo, Bunkyo-ku. Senior Member AIAA.
†Graduate Student, Department of Aeronautics and Astronautics, 7-3-1 Hongo, Bunkyo-ku.
‡Aerospace Research Associate, Next Generation Supersonic Transport Project Center, 6-13-1 Osawa, Mitaka.
§Senior Researcher, Next Generation Supersonic Transport Project Center, 6-13-1 Osawa, Mitaka.

Introduction

A LEADING-EDGE vortex flap is a full span deflectable surface at the leading edge of a delta wing.[1] With the flap deflected downward, a leading-edge separation vortex is formed over the forward-facing flap surface. The suction force generated by the vortex acts on the flap and generates a thrust component. Hence, it reduces the drag and improves the lift/drag (L/D) ratio, which is an essential factor for the improvement of the takeoff and climb performance of the delta wing aircraft such as a next generation supersonic transport. Many studies have confirmed the benefit of the vortex flap.[2–4]

Rinoie and Stollery,[5] Rinoie et al.,[6] Rinoie,[7] and Rinoie and Kwak[8] have made several experimental studies of vortex flaps for delta wing configurations. In these studies, the four main factors that affect the vortex flap characteristics (i.e. flap deflection angles),[5] wing sweepback angles,[6] leading-edge cross sections,[7] and flap hinge-line positions[8] are discussed. Throughout these studies, the effects of these four factors were discussed.

It is known for a plain delta wing with rounded leading edges that a large fraction of the leading-edge suction force acts on the rounded leading edge and reduces the drag component of the delta wing.[9–12] In Ref. 7 a combination of the vortex flaps and the rounded leading edge is examined. When the rounded leading-edge vortex flaps were deflected, suction forces, which are caused both by the leading-edge separation vortex over the flap surface and by the rounded leading edge, reduced the drag component and increased the lift/drag ratio. It was revealed in Ref. 7 that the 60-deg delta wing with the rounded-edged vortex flaps is more effective than the wing with sharp-edged vortex flaps when C_L is relatively high ($C_L > 0.4$).

Further studies have been conducted to clarify how the rounded leading-edge vortex flap improves the wing performance and are described here. The wing model tested has a cranked arrow wing that is used for a supersonic transport (SST) configuration. The vortex flap benefit on the SST configuration has been studied in Refs. 13–15. In these studies, the leading edge of the original wing, which was optimized for a supersonic cruise, was simply deflected as the vortex flap, or a sharp-edged thin flat plate was attached on the lower surface of the wing as the vortex flap; however, the effect of the flap cross section on the performance of the SST configuration has not been tested.

The wing configuration studied here is based on the cranked arrow wing configuration that was designed for a supersonic flight-test program currently underway by the National Aerospace Laboratory,

Japan.[16] The original designed cranked arrow wing was modified so that the leading edges can be deflected as leading-edge flaps. Two different leading-edge cross sections were tested, that is, the original design (relatively sharp leading edge) and the rounded leading edge, which has a diameter of 2% of the wing mean aerodynamic chord.

It has been pointed out that the performance of a rounded-edged delta wing is affected by the Reynolds number (see Ref. 11). In Ref. 7, tests were reported that were mainly conducted at a fixed single Reynolds number. In this paper, however, tests are conducted at several different Reynolds numbers to reveal the Reynolds number effect on the rounded leading-edge vortex flaps.

Here, a 2×2 m low-speed wind tunnel and a 2×2 m transonic wind tunnel were used for the tests. The force and surface pressure measurements were made on the described SST configuration model with different flap deflection angles and with different leading edges. Measurements at the 2×2 m low-speed wind tunnel were made in a range of angles of attack of from -4 to $+30$ deg at a Reynolds number based on the mean aerodynamic chord C_{mac} of 9.2×10^5. The performance of the vortex flap with the original leading edge has been investigated in this wind tunnel. Measurements at the 2×2 m transonic wind tunnel were made in a range of angles of attack from -3 to $+16$ deg at the Reynolds numbers between 1.5×10^6 and 3.8×10^6 at a freestream Mach number $M = 0.3$. The benefit of the rounded leading-edge vortex flaps and the effect of the Reynolds number on the rounded-edged vortex flaps were investigated in this wind tunnel.

In summary, the purpose of this study is to discuss the effect of the rounded leading-edge vortex flap for the SST configuration and to reveal the Reynolds number effect on the rounded leading-edge vortex flaps.

Experimental Details

Figure 1 shows the model details. This SST configuration model is based on the cranked arrow wing configuration with a fuselage section that was preliminary designed for the supersonic flight-test program conducted by the National Aerospace Laboratory. The wing has a sweepback angle of 66 deg at the inboard section and 42 deg at the outboard section. The kink is located between the inboard and outboard wings at $y/(b_{\max}/2) = 0.55$. The main wing was designed based on the supersonic lifting surface theory[17] at a design Mach number of 1.7, so that the wing has a warped wing section. The inboard wing has a thickness distribution of a NACA 66-series airfoil section with an average thickness chord ratio of 3%. The outboard wing has a biconvex airfoil section with a maximum thickness chord ratio of 3%. Details of the wing cross section are shown in Fig. 2.[18] The leading edge of this model was modified so that it has the vortex flaps on the inboard wing and leading-edge flaps on the outboard wing (Fig. 1). Because the sweepback angle of the inboard wing is large, the inboard leading-edge flap has been thought to act as the vortex flaps. The chord length of this inboard vortex flap is $0.1C_{\text{mac}}$. The chord length of the outboard leading-edge flap is 20% of the local chord length at each spanwise station. The vortex flap deflection angle δ_{fLEin} for the inboard wing is defined as the angle measured in the plane that is normal to the hinge line. The leading-edge flap deflection angle δ_{fLEout} for the outboard wing is defined as the angle measured parallel to the freestream. The tested flap deflection angles are $\delta_{\text{fLEin}} = 0$, 15, and 30 deg and $\delta_{\text{fLEout}} = 0$, 5, and 12.2 deg. The flaps have been designed so that there is no gap between the inboard leading-edge flap and the outboard leading-edge flap at the kink when $(\delta_{\text{fLEin}}, \delta_{\text{fLEout}}) = (15, 5 \text{ deg})$ and (30, 12.2 deg). Two rows of pressure tappings are located on the upper surface ($x/Cr = 0.55$ and 0.83). The nose section of the fuselage, that is, 25% of the total fuselage length, is an ogive–cone–cylinder.

Rounded leading-edge flap configurations were tested by modifying the lower surface of the leading edge of the inboard section of the original wing (Fig. 3). The flap deflection angle is the same as the original flap section $\delta_{\text{fLEin}} = 0$, 15, and 30 deg. It has a constant leading-edge diameter D of 0.01 m ($=0.02C_{\text{mac}}$)

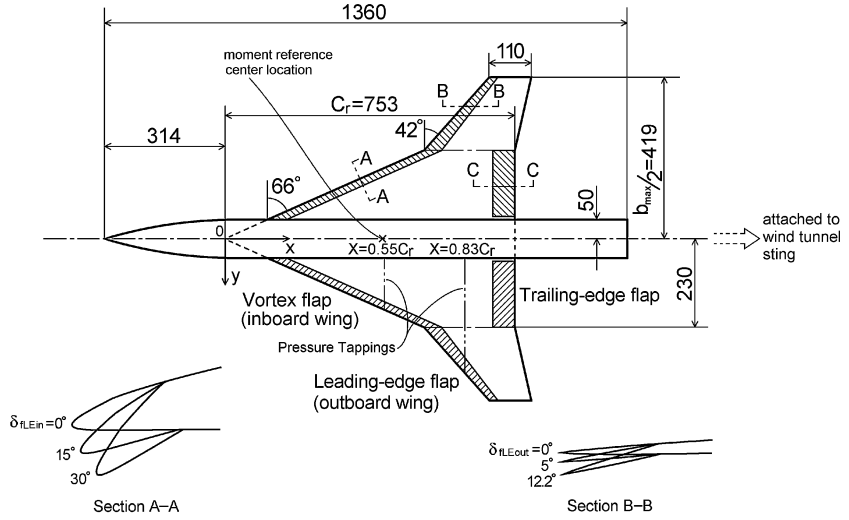

Fig. 1 SST model, in millimeters.

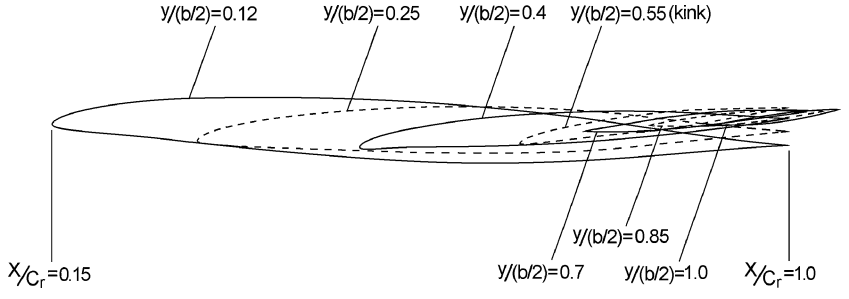

Fig. 2 Cross sections of original designed wing with vertical axis enlarged twice as long for clarity.

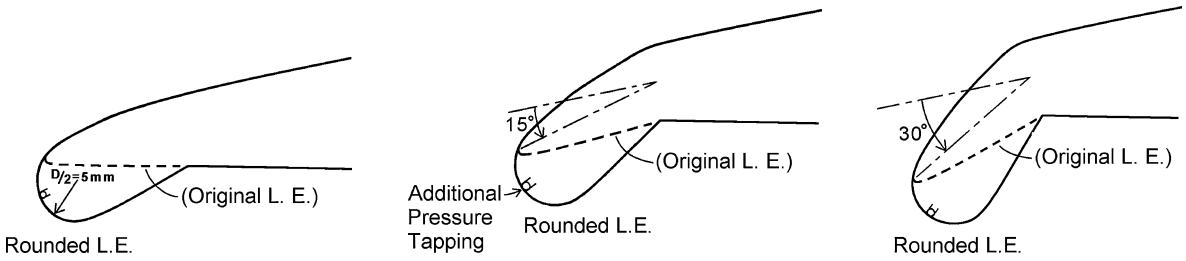

a) $\delta_{\mathrm{fLEin}} = 0$ **deg** **b)** $\delta_{\mathrm{fLEin}} = 15$ **deg** **c)** $\delta_{\mathrm{fLEin}} = 30$ **deg**

Fig. 3 Rounded leading edges (section A–A in Fig. 1).

between $y/(b_{\max}/2) = 0.21$ and 0.46. The diameter is defined in the plane that is normal to the leading-edge line (section A–A in Fig. 1). This diameter decreases linearly from $y/(b_{\max}/2) = 0.21$ toward $y/(b_{\max}/2) = 0.12$ and from $y/(b_{\max}/2) = 0.46$ toward $y/(b_{\max}/2) = 0.55$, so that the leading-edge configurations at $y/(b_{\max}/2) = 0.12$ and 0.55 coincide with the original wing design. Because the lower surface of the original wing was modified to have a rounded leading-edge section, the true flap deflection angle is greater than δ_{fLEin}, as can be seen in Fig. 3. Even when $\delta_{\mathrm{fLEin}} = 0$ deg for the rounded leading edge, the true flap deflection angle is about 12 deg. One additional pressure tapping is located at the leading edge of the rounded leading-edge section at $x/Cr = 0.55$ (Fig. 3).

The experiments were made in a 2×2 m low-speed wind tunnel and a 2×2 m transonic wind tunnel at the National Aerospace Laboratory, Japan. At the 2×2 m low-speed wind tunnel, tests were made at a tunnel speed of $U_\infty = 30$ m/s. The Reynolds number based on the mean aerodynamic chord ($C_{\mathrm{mac}} = 0.46$ m) was $Re = 9.21 \times 10^5$. The freestream turbulence intensity of the tunnel is about 0.06%. The angle of attack was in a range from -4 to $+30$ deg. Lift, drag, and the pitching moment were measured using a six-component internal balance. Surface pressure distributions were measured using electronic scanning pressure sensors (ESP). All of the aerodynamic coefficients were calculated based on the original wing area without any flap deflection. The effects of the Reynolds number were tested at the 2×2 m transonic wind tunnel using the same model. Tests were made at a tunnel speed of $M = 0.3$. By altering the wind-tunnel total pressure, tests at different Reynolds numbers have been conducted. Five different Reynolds numbers were tested ($Re = 1.44 \times 10^6$–3.83×10^6). The root mean square value of the pressure fluctuation in the tunnel is less than 1.1% when normalized by the freestream dynamic pressure. The angle of attack was in a range from -3 to $+16$ deg. Lift, drag, and the pitching moment were measured using a six-component internal balance. Surface pressure distributions were measured using a Scanivalve. The estimated overall accuracy of the aerodynamic coefficients is $\pm 1\%$ at 20:1 odds. The estimated overall accuracy of the pressure coefficient is $\pm 2\%$ at 20:1 odds.

Examples of the notation used in this paper are as follows. S301200 is the original wing with $\delta_{\mathrm{fLEin}} = 30$ deg and $\delta_{\mathrm{fLEout}} = 12$ deg. R150500 is the rounded leading edge with a flap deflection of $\delta_{\mathrm{fLEin}} = 15$ deg and $\delta_{\mathrm{fLEout}} = 5$ deg. The last two digits of this notation are reserved for the trailing-edge flap. The effects of the trailing-edge flap were also investigated using the same model, and the results are described in Ref. 18.

Flap Performance of Original Wing

In this section, the performance of the original wing with flap deflection is briefly discussed. Figures 4a–4d show the lift, drag, pitching moment, and lift/drag curves at $Re = 9.21 \times 10^5$. Figures 4a and 4b show the results for the original SST configuration with no flap deflection (S000000), the configuration of the inboard vortex flap deflection $\delta_{\mathrm{fLEin}} = 15$ deg (S150000), that of the outboard leading-edge flap deflection $\delta_{\mathrm{fLEout}} = 5$ deg (S000500), and finally for the combinations of the vortex flap $\delta_{\mathrm{fLEin}} = 15$ deg and the leading-edge flap deflections $\delta_{\mathrm{fLEout}} = 5$ deg (S150500).

The C_L vs α curves in Fig. 4a show that the vortex flap and leading-edge flap deflections (S150000, S000500, and S150500) slightly decrease C_L as compared with S000000, especially when α is greater than 10 deg. The C_D vs α curves in Fig. 4b show that C_D decreases as compared with S000000 when the vortex flap and the leading-edge flap are deflected. The C_m vs C_L curves in Fig. 4c show that C_m is slightly affected by the flap deflection, except when S000500. References 5–8 indicated that the vortex flap has little effect on C_m for the delta wings. The plan shapes of the wing and the flaps are different between the present cranked arrow configuration and the delta wings in Refs. 5–8. This may be the reason for the different behavior of C_m. Note that the C_m was measured about $0.25C_{\mathrm{mac}}$ in this paper, although the C_m of the delta wing configuration is often referenced to $0.5C_{\mathrm{mac}}$ for stability and control analyses.

Figure 4d shows the lift to drag ratio (L/D) vs C_L. Figure 4d shows that the vortex flap deflection (S150000) has some benefit when $C_L = 0.2$–0.6 as compared with that of S000000. The results of the outboard leading-edge flap (S000500) indicate that the L/D is slightly improved for S000500 between $C_L = 0.15$ and 0.6. The maximum value of L/D is also improved as compared with that of S000000. However, these results are not so encouraging as compared with those of the delta wing with the vortex flaps reported in Refs. 5–8.

When the vortex flaps and the leading-edge flaps are deflected at the same time (S150500), a higher benefit can be seen in the C_L range between 0.2 and 0.7. The percentage increase in L/D for S150500 as compared with the S000000 is about 12% between $C_L = 0.25$ and 0.5. The combined use of the vortex flaps and the leading-edge flaps shows some benefit for the performance of the SST configuration. It has been reported in Ref. 15 that the C_L range at SST's takeoff is between 0.4 and 0.6. Similarly, a C_L of approximately 0.4–0.5 will be used here to discuss the flap performance at takeoff.

Figure 5 shows the surface pressure distributions for the same flap configurations as in Fig. 4, in the spanwise direction for the upper surface at $x/Cr = 0.55$ and 0.83 when $\alpha = 5$ and 10 deg. Figure 5a indicates that the vortex flap (S150000) suppresses the separation over the flap surface at a relatively low angle of attack ($\alpha = 5$ deg) at $x/Cr = 0.55$. This agrees with the observation reported in Ref. 5. Figure 5c ($\alpha = 10$ deg, at $C_L \cong 0.4$) indicates that, as for S150000, the spanwise length of the separated region at $x/Cr = 0.55$ is reduced as compared with S000000, and the location of this separated region is confined mainly on the vortex flap surface. This confirms the description made in the second section that the inboard flap deflection (S150000) works as the vortex flap, and thus, the L/D has slightly been improved at $C_L \cong 0.4$ as was shown in Fig. 4d.

As for the outboard leading-edge flap configuration (S000500), Fig. 5b ($\alpha = 5$ deg, $C_L \cong 0.2$) shows that the separation is suppressed at $x/Cr = 0.83$. This suppression may have improved the L/D at $C_L \cong 0.2$ as was shown in Fig. 4d. Figure 5d ($\alpha = 10$ deg, at $C_L \cong 0.4$) indicates that as for S000500 there are two suction peaks at $x/Cr = 0.83$. The first suction observed on the flap surface is caused by the separation at the leading edge of the outer leading-edge flap. The second suction peak is observed near the kink station [$y/(b/2) = 50$–70%]. Because the suction peak near the kink is also observed on S000000 in Fig. 5, this suction is thought to be caused by the separation from the kink or the inboard wing section.

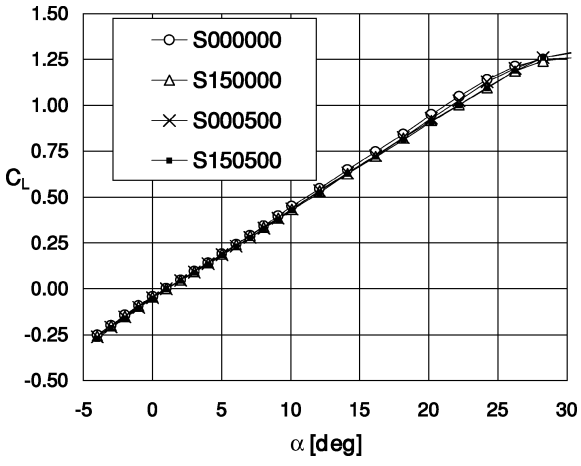

a) C_L–α

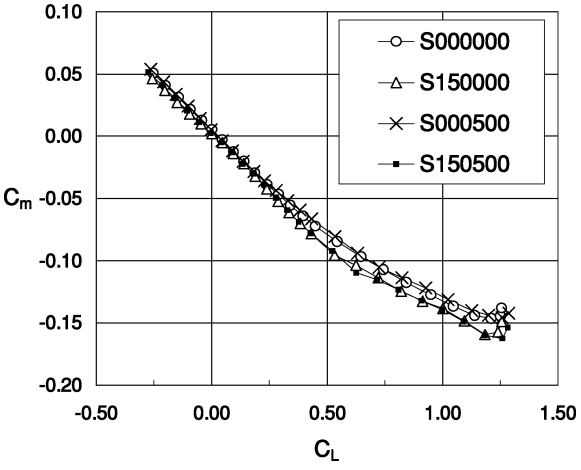

c) C_m–C_L

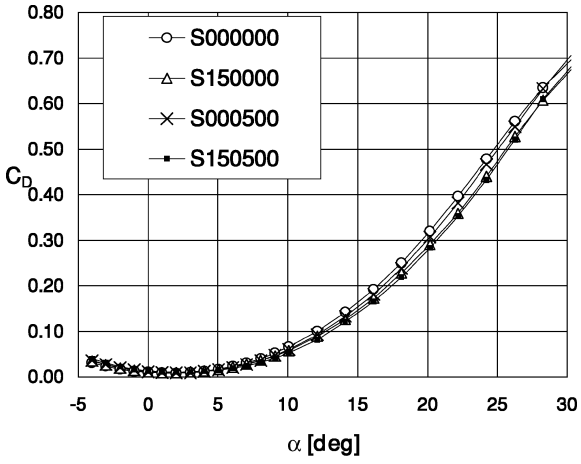

b) C_D–α

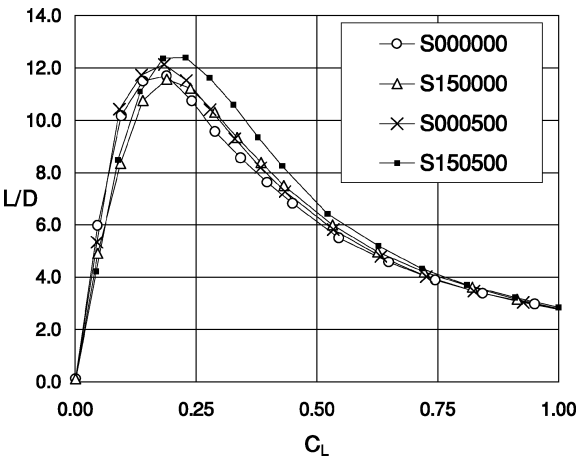

d) L/D–C_L

Fig. 4 Effects of vortex flaps and leading-edge flaps for original leading-edge, force measurements, $Re = 9.21 \times 10^5$.

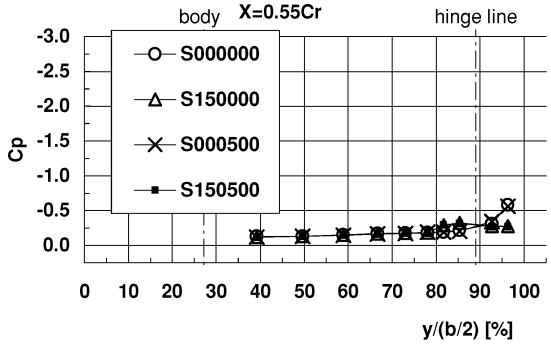

a) $\alpha = 5$ deg, $x = 0.55Cr$

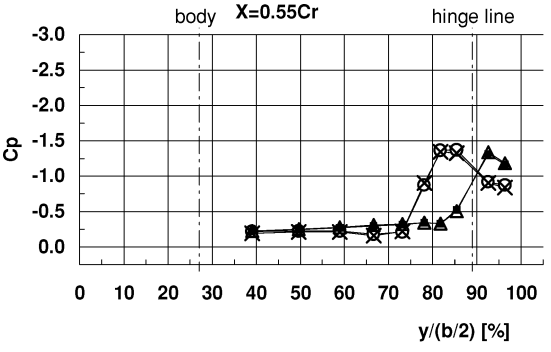

c) $\alpha = 10$ deg, $x = 0.55Cr$

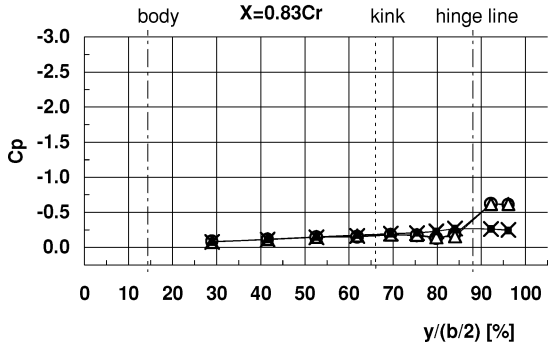

b) $\alpha = 5$ deg, $x = 0.83Cr$

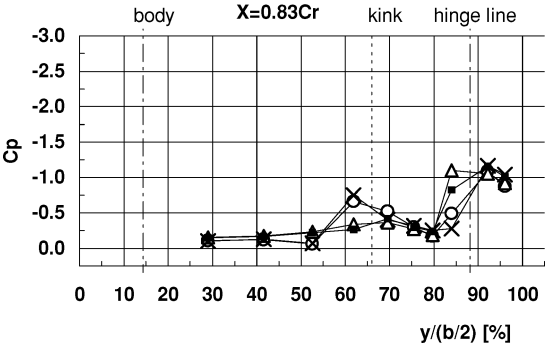

d) $\alpha = 10$ deg, $x = 0.83Cr$

Fig. 5 Effects of vortex flaps and leading-edge flaps for original leading-edge, surface pressure measurements, $Re = 9.21 \times 10^5$.

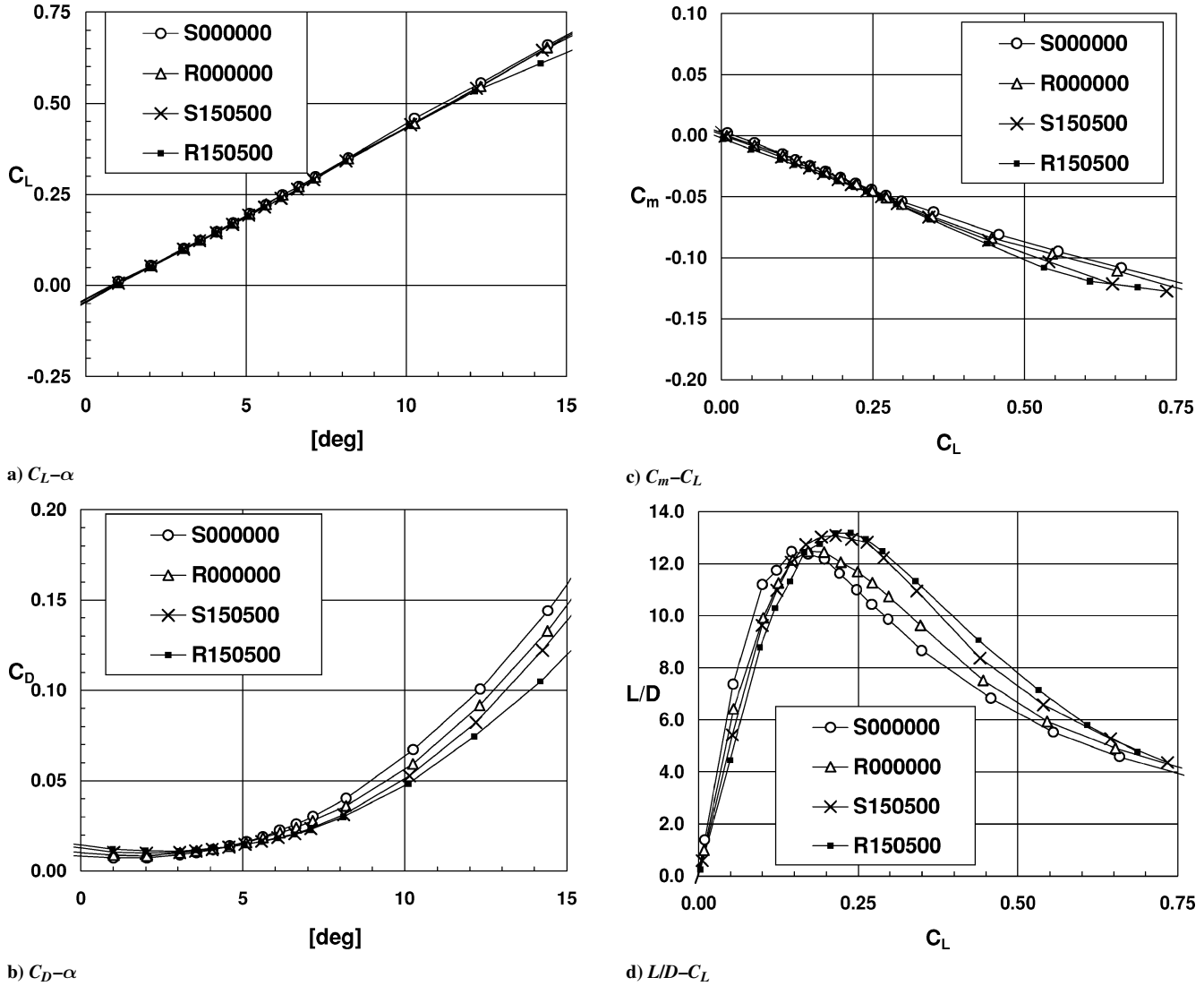

a) C_L–α c) C_m–C_L

b) C_D–α d) L/D–C_L

Fig. 6 Effects of rounded leading edge with and without flap deflection, force measurements, $Re = 3.41 \times 10^6$.

When the inboard vortex flaps and the outboard leading-edge flaps are deflected at the same time (S150500), Figs. 5a and 5c show that at $x/Cr = 0.55$ the pressure distribution of this configuration is quite similar to that of S150000. This means that S150500 is working as the vortex flap at $x/Cr = 0.55$ when $\alpha = 10$ deg. At $x/Cr = 0.83$, the C_p distributions in Fig. 5d indicate that the S150500 behaves like S150000 at the inboard section near $y/(b/2) = 50$–70%. (Note that the suction region near the kink at $\alpha = 10$ deg is not observed that was seen in S000500.) This may have helped to reduce the drag. For these reasons, the combination of the inboard vortex flaps and the outboard leading-edge flaps improves the L/D as was seen in Fig. 4d.

Tests at $\delta_{\text{fLEin}} = 30$ and $\delta_{\text{fLEout}} = 12.2$ deg were also conducted. The results of S301200 indicated characteristics similar to those of S150500.

Effects of Rounded Leading Edge

Figure 6 shows the lift, drag, pitching moment, and lift/drag curves when the wing has an inboard rounded leading edge with and without flap deflection (R000000 and R150500) together with the results from the original wing (S000000 and S150500) at $Re = 3.41 \times 10^6$. When the inboard vortex flap was deflected 15 deg, the outboard leading-edge flap was also deflected 5 deg to minimize the gap between these flaps. The lift to drag ratio (L/D) vs the C_L curve indicates that R000000 shows better L/D ratios than does S000000 when C_L values are greater than 0.2. A suction effect of the rounded leading edge is demonstrated. The rounded leading-edge vortex flaps (R150500) also indicate better L/D ratios when compared with those of S150500 when $C_L > 0.3$. The percentage increase in L/D for R150500 as compared with S000000 is about 27% at $C_L = 0.4$ at this Reynolds number. These results confirm the benefit of the rounded leading-edge vortex flaps as in Ref. 7.

Figure 7 shows surface pressure distributions at $x/Cr = 0.55$ for these four configurations at $\alpha = 8$, 10, and 12 deg. The formation of the leading-edge separation vortex is observed for most of the configurations. Figures 7 indicate that, as the leading-edge radius is increased (S000000 → R000000 and S150500 → R150500), the spanwise length of the suction region is reduced. A similar trend was seen in Ref. 7.

Experiments with a 30-deg inboard vortex flap deflection (R301200) were also conducted. However, nothing beneficial was observed as compared with those of S301200. This may be explained by the drag increase due to the flow separation occurring underneath the flap because of a high deflection angle at the lower surface of the rounded-edged flap (Fig. 3c).

Effects of Reynolds Numbers on Rounded Leading Edge

Figure 8 shows the C_p distributions ($\alpha = 12$, 14, and 16 deg at $x/Cr = 0.55$) when the Reynolds number is increased for the original (NACA 6-series nonrounded) leading-edge wing with flap deflection (S150500). The C_p distributions in Figure 8 show only a

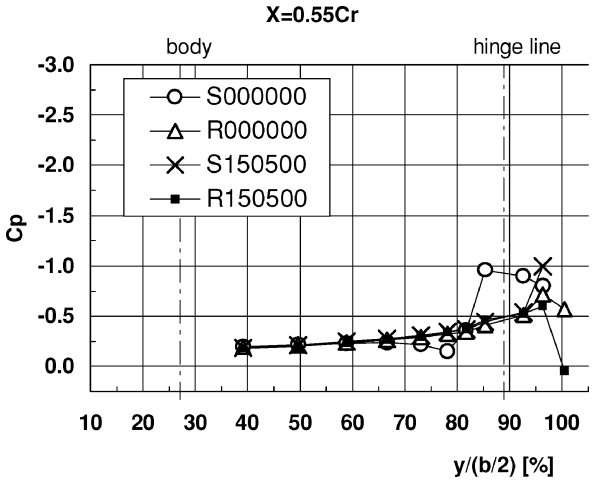

a) $\alpha = 8$ deg

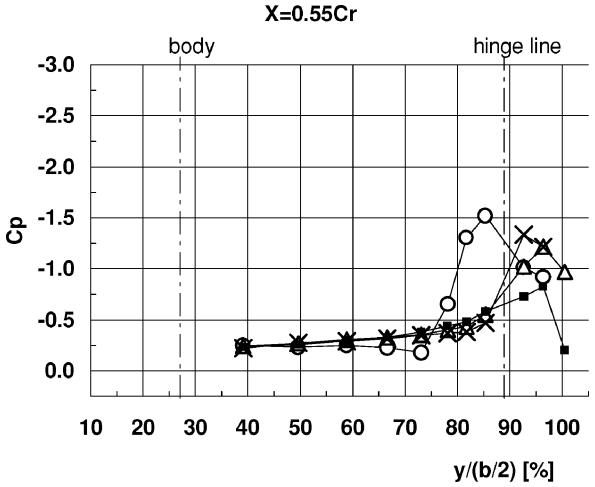

b) $\alpha = 10$ deg

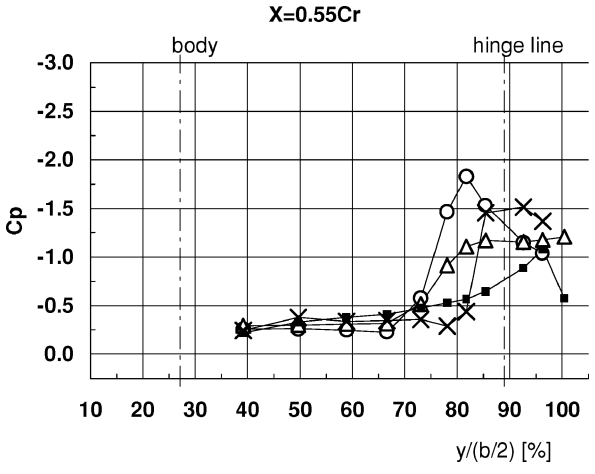

c) $\alpha = 12$ deg

Fig. 7 Effects of rounded leading edge with and without flap deflection, surface pressure, $Re = 3.41 \times 10^6$.

small difference in the cases at different Reynolds numbers. This clearly indicates that the flow around S150500 is not affected by the Reynolds numbers.

Figures 9a and 9b show the L/D and the axial force coefficient C_A distributions at different Reynolds numbers for the rounded leading-edge wing (R150500). C_A is defined by

$$C_A = C_D \cos\alpha - C_L \sin\alpha$$

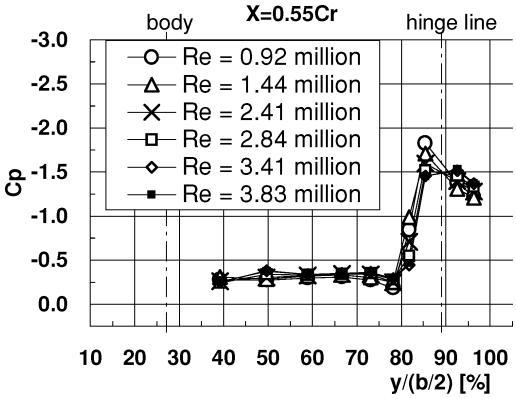

a) $\alpha = 12$ deg

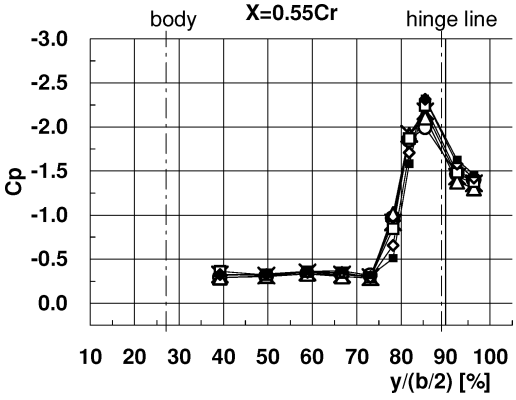

b) $\alpha = 14$ deg

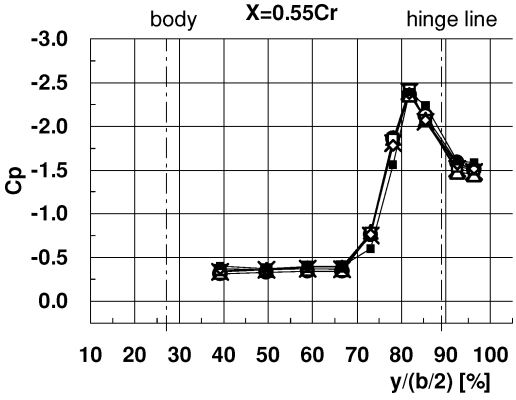

c) $\alpha = 16$ deg

Fig. 8 Effects of Reynolds number on original leading-edge wing, surface pressure, S150500.

The negative value of C_A is caused by the leading-edge suction force and by the suction pressure acting on the positive slope area on the upper rounded surface of the deflected flap. Although a high L/D benefit was expected as the Reynolds number is increased, the L/D distributions in Fig. 9a show only a small increase in L/D. The C_A distributions in Fig. 9b also show that the C_A is not very affected by the difference in the range of the tested Reynolds numbers. However, the C_p distributions at different Reynolds numbers for R150500 in Fig. 10 indicate that, as the Reynolds number is increased, the suction peak decreases and the spanwise length of the suction region is reduced especially at $\alpha = 14$ and 16 deg. As noted before, different Reynolds numbers were achieved by varying the wind-tunnel total pressure. Because the cranked arrow wing has a swept elastic axis, the outboard wing panel deflects upward with increasing load from increasing dynamic pressure. Therefore,

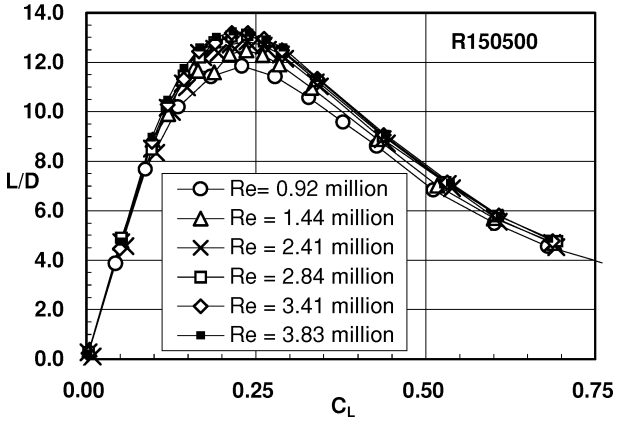

a) L/D–C_L

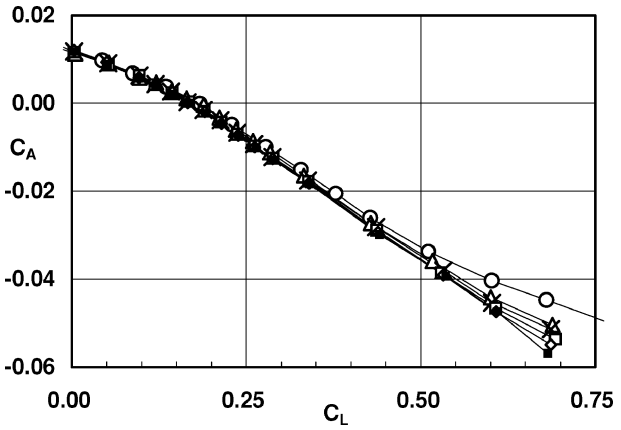

b) C_A–C_L

Fig. 9 Effects of Reynolds number on rounded leading edge, L/D–C_L and C_A–C_L, R150500.

the data presented in Fig. 9 may be affected by the local twisting deformation of the outboard wing panel such that Fig. 9 shows a combined Reynolds number and static aeroelastic effects. However, surface pressure distributions at $x/Cr = 0.55$ presented in Figs. 8 and 10 are far enough inboard that they may not be affected by these static aeroelastic effects because the inboard wing is thicker and does not twist as much as the outboard wing.

To see clearly the flow pattern changes when the Reynolds number is increased, crossflow patterns over the flap surface are shown for certain α and Reynolds number in Figs. 11 (S150500) and 12 (R150500). Crossflow patterns are deduced from the surface pressure measurements at $x/Cr = 0.55$. The angles of attack α, when the L/D attains its local maximum for a constant Reynolds number and when the C_L equals about 0.5 are specifically indicated in Figs. 11 and 12. Typical flow patterns and the examples of corresponding pressure distribution are also shown. Figure 11 shows that as for S150500 the flow in the crossflow planes at $x/Cr = 0.55$ can be divided into three different regimes. First, in regime A, the leading-edge separation vortex is not formed or only a small separation bubble is formed at the leading edge. Second, in regime B, the leading-edge separation vortex is formed over the flap surface. Third, in regime C, a large separation vortex is formed, and its reattachment line is located inboard of the flap hinge line. Figure 11 also shows that the α, where the boundary between these three regimes lies, are almost identical for different Reynolds numbers. This agrees with Fig. 8, where the Reynolds number tested here does not affect the flow over S150500.

Figure 12 indicates the crossflow pattern distributions for R150500. Here, the flow is divided into four different regimes. Regimes A and C are the same as in Fig. 11. However, regime B in Fig. 12 is divided into two regimes (B-1 and B-2). Regime

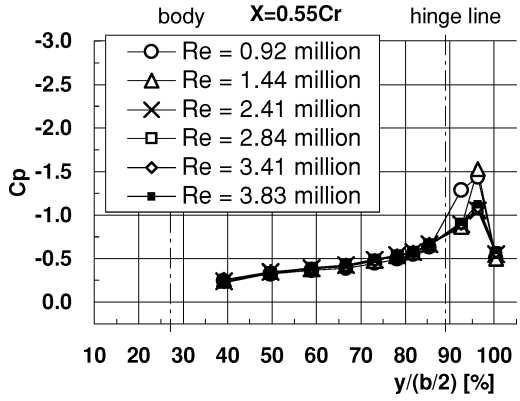

a) $\alpha = 12$ deg

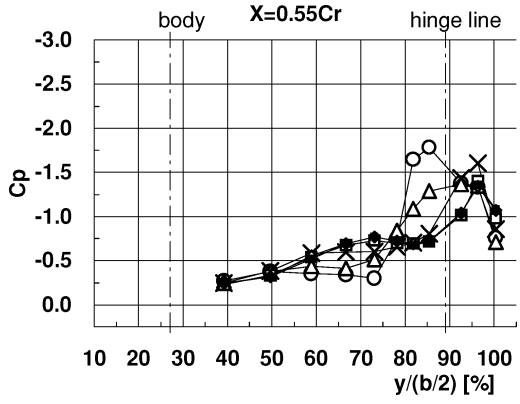

b) $\alpha = 14$ deg

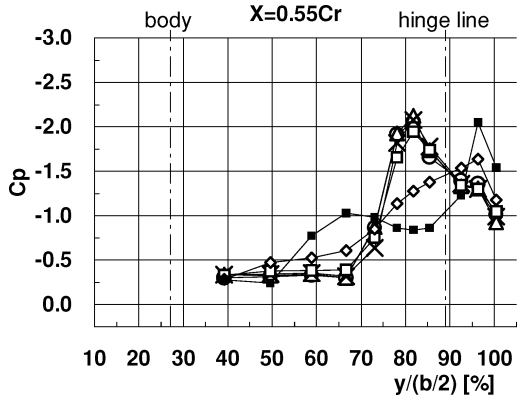

c) $\alpha = 16$ deg

Fig. 10 Effects of Reynolds number on rounded leading edge, surface pressure, R150500.

B-1 in Fig. 12 corresponds to regime B in Fig. 11. In regime B-2, the leading-edge separation vortex is formed on the flap surface as in regime B-1. However, inboard of the flap hinge line, the C_p distributions indicate that there is a small suction region. This may indicate that the flow separation also occurs inboard of the flap hinge line. However, because the suction pressure is very small and the dominant flow pattern is the leading-edge separation vortex on the flap surface, we have named this region B-2, a kind of derivation from regime B-1. Figure 12 indicates that, as the Reynolds number is increased, the α where the boundary between regime C and B-2 increases in the α axis when $Re > 2.5 \times 10^6$. This corresponds to the flow observed in Fig. 10, where the flow pattern changes as the Reynolds number is increased. The Reynolds number effect is observed at a higher Reynolds number and a higher α ($C_L > 0.5$). However, as was seen in Fig. 9, this flow pattern change has only a small influence on the wing lift/drag ratio itself in this test.

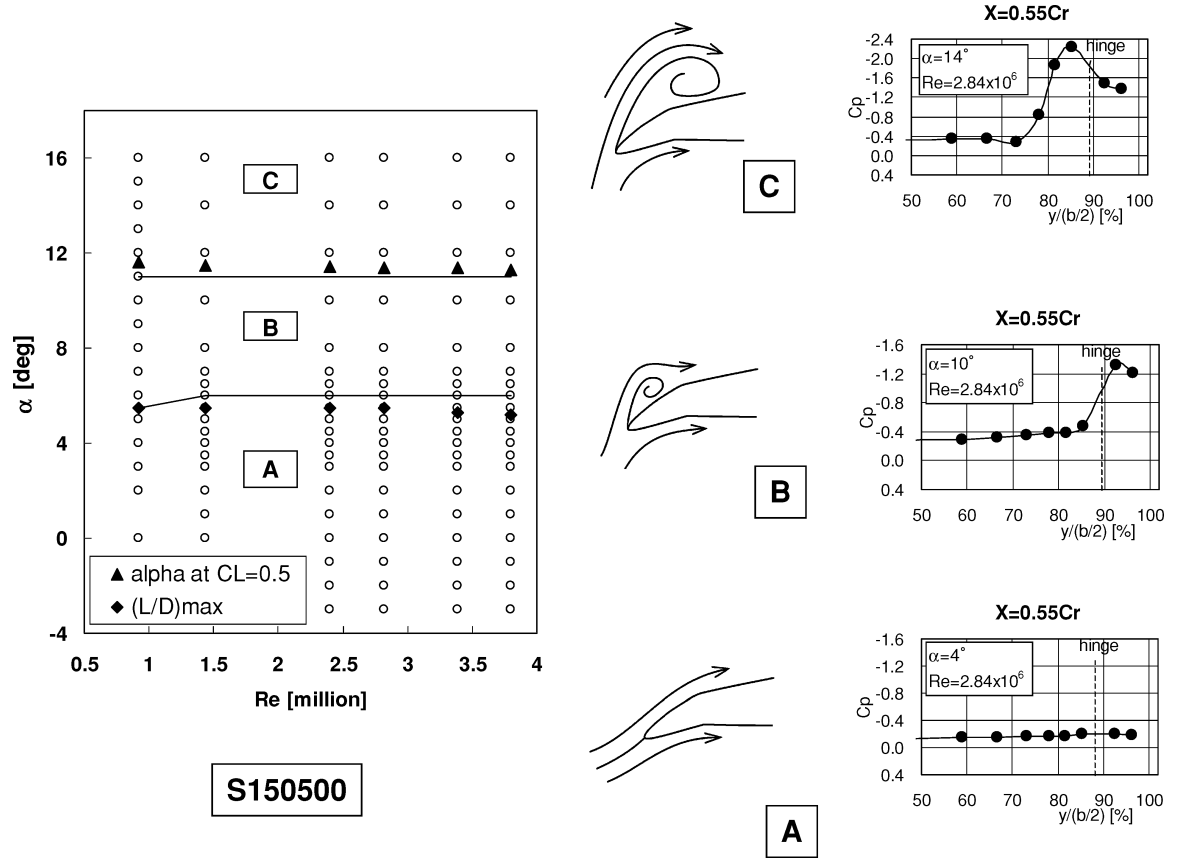

Fig. 11 Crossflow patterns at different Reynolds numbers for S150500.

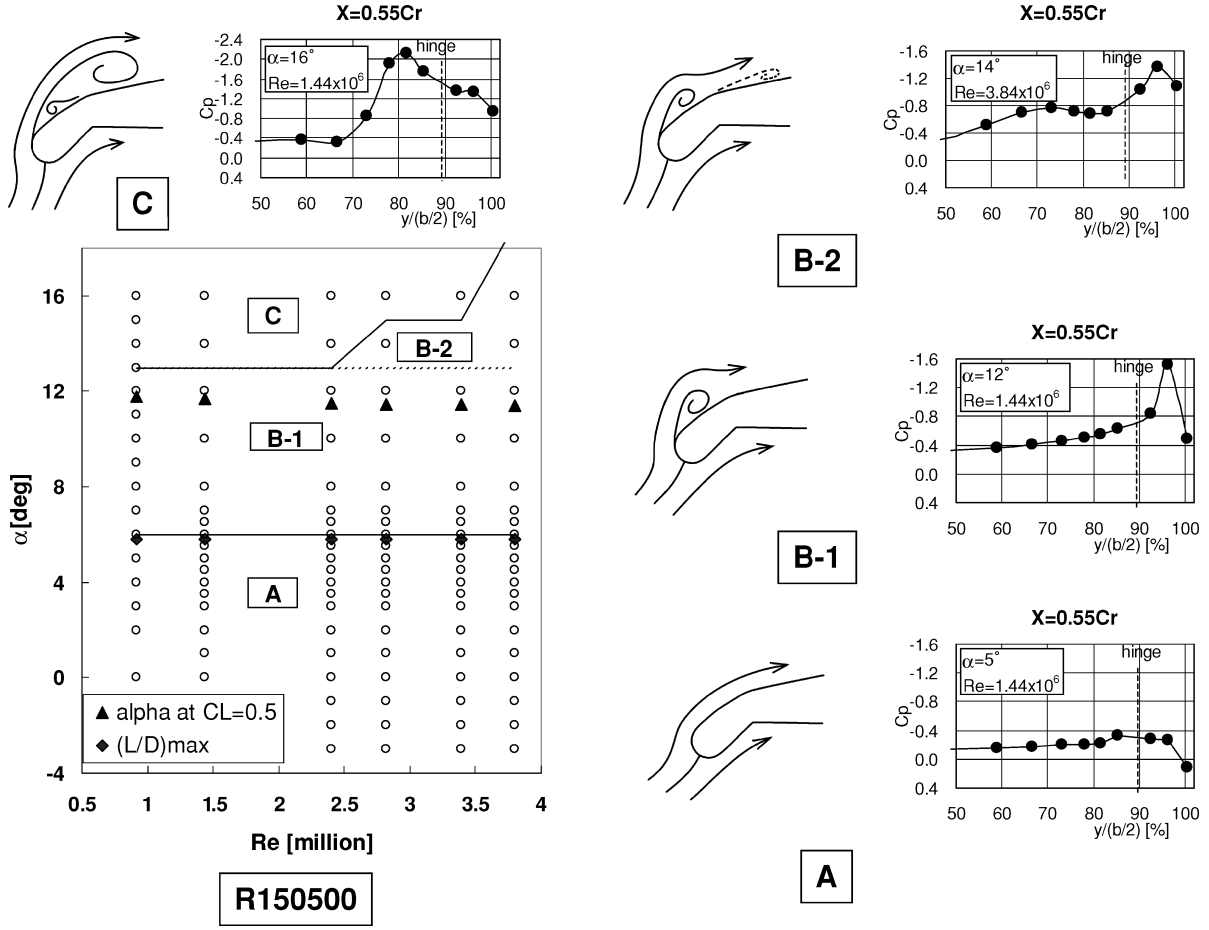

Fig. 12 Crossflow patterns at different Reynolds number for R150500.

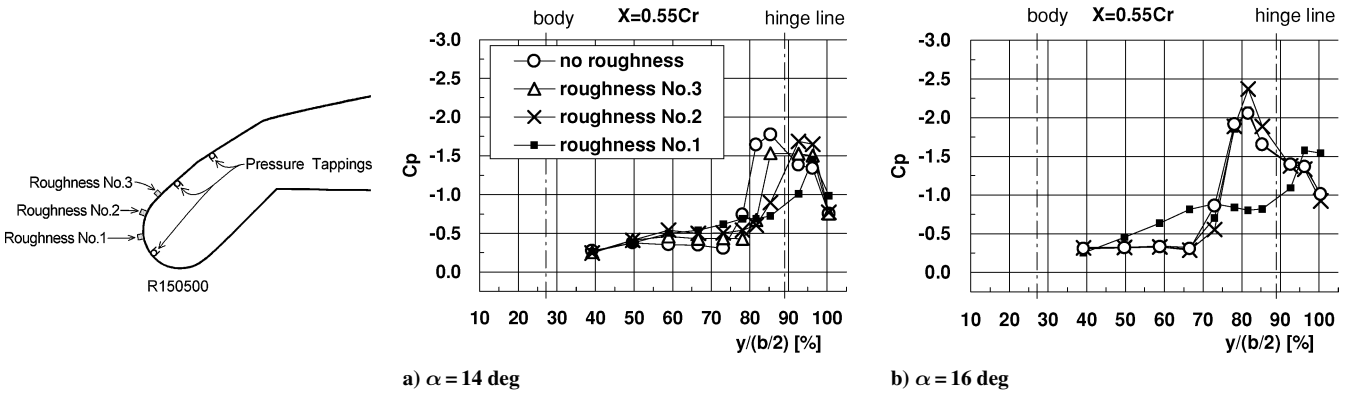

Fig. 13 Effects of surface roughness, surface pressure, R150500, $Re = 9.21 \times 10^5$.

Effects of Surface Roughness on Rounded Leading Edge

It has been thought that the reason for the Reynolds number effects observed in the preceding section is the difference of the boundary-layer transition position and the subsequent reduction of the separation region over the flap surface. Therefore, supplementary tests were made at the 2×2 m low-speed wind tunnel ($Re = 9.21 \times 10^5$) to examine the Reynolds number effect by adding roughness to the leading edge of the upper surface of the model with a rounded leading edge (R150500). The roughness used was an adhesive thin strip 0.15 mm thick and 1 mm wide. These strips were attached at three different positions separately, positions 1, 2 and 3, that is, roughness 1 was 4 mm from the leading-edge, roughness 2 was 8 mm, and roughness 3 was 12 mm (Fig. 13). The strips located at roughness position 1 would be sufficient to cause transition to turbulent flow at the tested Reynolds number, according to the estimation method based on Ref. 19 if the flow is a two-dimensional boundary layer over the flat plate. The main focus of roughness was to see the sensitivity of the results to the Reynolds number by simulating the turbulent boundary layer that is expected at a higher Reynolds number.

Figure 13 shows the surface pressure distributions for R150500 at $\alpha = 14$ and 16 deg with roughnesses 1–3 and also without roughness. Figure 13 indicates that as the roughness position moves toward the leading edge (position 3 −> position 1), the spanwise length of the suction region becomes shorter. When the data in Fig. 13 are compared with those in Fig. 10 that were measured at different Reynolds numbers, Figs. 13 and 10 show quite similar distributions at $\alpha = 14$ and 16 deg. This suggests that the transition point on the flap surface may have moved either when the roughness position is changed or when the Reynolds number is increased. However, the flow characteristics over the flap surface, that is, laminar or turbulent flow, were not measured in this study. To make the preceding discussion clearer, more detailed flow measurements are necessary. Because the flow considered here is the one around the rounded leading edge of a sweptback wing, it is thought that the flow is affected by a crossflow instability.

Note that the rounded leading edge may be used for the inboard wing leading edge such as the present model when flying at supersonic speed because the inboard leading edges are by design swept enough to have the flow normal to the leading edge remain subsonic even when the aircraft is flying at supersonic cruise conditions. However, the rounded leading edge for the outboard wing can only be used when flying at low speed because of a high wave drag penalty at supersonic speeds.

Conclusions

Wind-tunnel measurements were taken on a cranked arrow wing SST configuration. Two different flap cross sections (originally designed NACA 6-series nonrounded leading edge and the rounded leading edge) were tested. The purpose of the measurements is to clarify how the differences of the Reynolds number affect the flow around the rounded leading-edge vortex flaps and the flap performance.

1) The combination of the nonrounded vortex flaps at the inboard wing and the leading-edge flaps at the outboard wing shows a lift/drag ratio benefit in the lift coefficient range of 0.2–0.7 as compared with the wing without flap deflections.

2) The rounded leading-edge vortex flaps indicate some benefit of the lift/drag ratio as compared with those of nonrounded vortex flaps at a relatively high-lift coefficient greater than 0.3.

3) Different flow patterns were observed over the rounded leading-edge vortex flaps when the Reynolds number is increased at lift coefficient greater than 0.5. At a lower Reynolds number, a separation vortex that has a relatively long spanwise length is formed. When the Reynolds number is increased, the spanwise length of the separated region shortens.

References

[1]Rao, D. M., "Leading Edge Vortex-Flap Experiments on a 74deg. Delta Wing," NASA CR-159161, Nov. 1979.

[2]Marchman, J. F., III, "Effectiveness of Leading-Edge Vortex Flaps on 60 and 75 Degree Delta Wings," *Journal of Aircraft*, Vol. 18, No. 4, 1981, pp. 280–286.

[3]Frink, N. T., "Subsonic Wind-Tunnel Measurements of a Slender Wing–Body Configuration Employing a Vortex Flap," NASA TM-89101, July 1987.

[4]Levin, D., and Seigner, A., "Experimental Investigation of Vortex Flaps on Thick Delta Wings," *Journal of Aircraft*, Vol. 31, No. 4, 1994, pp. 988–991.

[5]Rinoie, K., and Stollery, J. L., "Experimental Studies of Vortex Flaps and Vortex Plates," *Journal of Aircraft*, Vol. 31, No. 2, 1994, pp. 322–329.

[6]Rinoie, K., Fujita, T., Iwasaki, A., and Fujieda, H., "Experimental Studies of a 70-Degree Delta Wing with Vortex Flaps," *Journal of Aircraft*, Vol. 34, No. 5, 1997, pp. 600–605.

[7]Rinoie, K., "Experiments of a 60-Degree Delta Wing with Rounded Leading-Edge Vortex Flaps," *Journal of Aircraft*, Vol. 37, No. 1, 2000, pp. 37–44.

[8]Rinoie, K., and Kwak, D. Y., "Studies on Vortex Flaps Having Different Flap Hinge-Line Positions," *Journal of Aircraft*, Vol. 38, No. 2, 2001, pp. 396–398.

[9]Jones, R., Miles, J. W., and Pusey, P. S., "Experiments in the Compressed Air Tunnel on Swept-Back Wings Including Two Delta Wings," British Aeronautical Research Council (ARC) Reports and Memoranda 2871, London, 1954.

[10]Fletcher, H. S., "Low-Speed Experimental Determination of the Effects of Leading-Edge Radius and Profile Thickness on Static and Oscillatory Lateral Stability Derivatives for a Delta Wing," NACA TN-4341, July 1958.

[11]Henderson, W. P., "Effects of Wing Leading-Edge Radius and Reynolds Number on Longitudinal Aerodynamic Characteristics of Highly Swept Wing–Body Configurations at Subsonic Speeds," NACA TN D-8361, Dec. 1976.

[12]Chu, J., and Luckring, M., "Experimental Surface Pressure Data Obtained on 65° Delta Wing Across Reynolds Number and Mach Number Ranges," NASA TM 4645, Feb. 1996.

[13]Yip, L., and Murri, D. G., "Effects of Vortex Flaps on the Low-Speed Aerodynamic Characteristics of an Arrow Wing," NASA TP 1914, Nov. 1981.

[14]Coe, P. L., Jr., Kjelgaard, S. O., and Gentry, G. L., Jr., "Low-Speed Aerodynamic Characteristics of a Highly Swept, Untwisted, Uncambered Arrow Wing," NASA TP 2176, Oct. 1983.

[15]Nicholls, K. P., "Flap Systems on Supersonic Transport Aircraft," *Proceedings of the Confederation of European Aerospace Societies (CEAS) European Forum on High Lift and Separation Control*, The Royal Aeronautical Society, London, 1995, pp. 3.1–3.6.

[16]Sakata, K., "Supersonic Experimental Airplane (NEXST) for Next Generation SST Technology—Development and Flight Test Plan for the Unmanned Scaled Supersonic Glider," AIAA Paper 2002-0527, Jan. 2002.

[17]Carlson, H. W., and Miller, D. S., "Numerical Method for the Design and Analysis of Wings at Supersonic Speeds," NASA TN D-7713, Dec. 1974.

[18]Kwak, D. Y., Miyata, K., Noguchi, M., Sunada, Y., and Rinoie, K., "Experimental Investigation on High Lift Devices for an SST," National Aerospace Laboratory of Japan, Tokyo, Technical Rept. NAL-TR-1450, Oct. 2002 (in Japanese).

[19]Schlichting, H., *Boundary-Layer Theory*, 7th ed., McGraw–Hill, New York, 1979, pp. 538–542.